




Comparison of X-ray Computed Tomography and Ultrasonic C-Scan Techniques and Numerical Modelling of Impact Damage in a CFRP Composite Laminate

E. E. Evans¹ · R. A. Brooks² · J. Liu² · Z. E. C. Hall² · H. Liu³ · T. J. E. Lowe¹ · P. J. Withers¹ · A. J. Kinloch² · J. P. Dear² 

Received: 15 August 2023 / Accepted: 4 October 2023 / Published online: 8 November 2023
© The Author(s) 2023

Abstract

Two different experimental techniques are employed to visualize the impact damage generated by a low-velocity impact on a carbon-fibre reinforced-polymer (CFRP) composite laminate. At the relatively low impact-velocity of 1.69 m.s^{-1} , and a corresponding impact energy of 7.5 J , used in the present work the damage induced in the CFRP panel is barely visible to the naked eye but the techniques of ultrasonic C-scan and X-ray computed tomography (CT) can detect the damage that has occurred. This damage is mostly inter-laminar damage, i.e. delaminations, between the plies due to a change in modulus from one ply to the next in the laminate. This interlaminar damage is usually accompanied by intralaminar damage, e.g. matrix cracking, in the ply itself. The type and extent of damage detected from using these two techniques is discussed and the relative merits of these techniques are compared. In general, the CT gave the better resolved picture of damage but the lateral extent of the damage was underestimated relative to C-scan which was more sensitive to very fine delamination cracks. In addition, a numerical approach, based on a finite-element analysis model, is employed to predict the type, location and extent of damage generated by the impact event and the modelling predictions are compared to the experimental results.

Keywords CFRP composite · Barely Visible Impact Damage (BVID) · Ultrasonic C-scan · X-ray computed tomography (CT) · FEA damage model

✉ E. E. Evans
elizabeth.evans-5@manchester.ac.uk

✉ J. P. Dear
j.dear@imperial.ac.uk

¹ Department of Materials, Henry Royce Institute and Henry Moseley X-ray Imaging Facility, University of Manchester, Manchester M13 9PL, UK

² Department of Mechanical Engineering, Imperial College London, South Kensington Campus, London SW7 2BX, UK

³ School of Engineering and Materials Science, Queen Mary University of London, London E1 4NS, UK

1 Introduction

Compared to more traditional metallic materials, carbon-fibre reinforced-polymer (CFRP) composites possess excellent stiffness-to-weight and strength-to-weight ratios. Further, they demonstrate very good environmental resistance and cyclic-fatigue properties. Therefore, they are widely used in the latest generation of passenger aircraft for fuselage, wings, engine cowls, ailerons and spoilers [1–3]. However, during manufacture and service, these structures are vulnerable to damage caused by impact events, such as dropped tools, foreign object damage and runway debris [2, 4–6]. In some cases, the impact damage can be extensive, in other cases the damage can be what is termed ‘barely visible impact damage (BVID)’ [6].

The major damage mechanisms observed [e.g. 7–10] when a CFRP composite is impacted at a relatively low-velocity (of up to about 5 m.s^{-1}) are: (a) intralaminar damage which typically involves plastic deformation of the matrix, matrix cracking, fibre debonding and localised fibre failure and (b) interlaminar damage which typically involves the initiation and growth of delaminations between the layers, i.e. plies, that form the composite laminate. These main damage mechanisms are illustrated in Fig. 1.

Ultrasonic C-scan imaging is one the most widespread Non-Destructive Testing (NDT) techniques used to detect interlaminar delaminations, i.e. interlaminar cracking. The C-scan equipment has a phased-array probe integrated with pulsars/receivers. The probe is also equipped with an encoder to provide the position of the probe along the scan axis. Ultrasonic waves with frequencies ranging from 0.5 to 50 MHz are typically transmitted through the composite to be tested and, upon encountering a delamination in the composite, the waves are reflected back to the transducer. Ultrasonic C-scan inspection methods are very good at detecting interlaminar cracks, if they are suitably oriented to reflect the ultrasound [11]. However, whilst ultrasonic C-scan testing is sensitive to delaminations, it is typically insensitive to the relatively small-scale intralaminar cracking damage [12].

X-ray computed tomography (CT) technique can provide perhaps the most informative view of damage in 3-D NDT [12]. In contrast to ultrasonics, the resolution of the CT, which can achieve micro or even sub-micron scales (hence, ‘micro-CT’), can provide detailed information about the nature of the damage. For example, it has been used to distinguish and quantify the evolution of matrix cracking, cracks in resin-rich areas and ply-by-ply delaminations [13, 14]. In most cases, the damage is categorised and visualised using automated or semi-automated segmentation methods [15] to distinguish the different types of damage in terms of the attenuation of the grey scales and morphology, but this is often difficult for

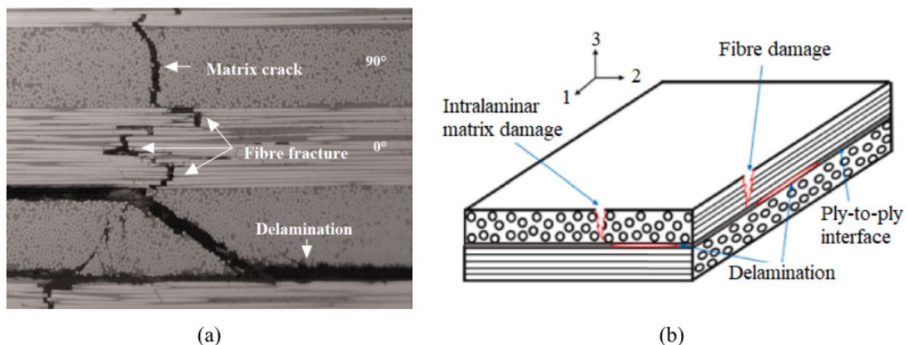


Fig. 1 Different types of damage in a composite laminate subjected to an impact load [10]

CFRP composites because of the contrast between the fibres, the matrix and the damage can be low. Furthermore, the crack or delamination may be narrower than a voxel (i.e. a 3-D pixel) meaning that it is not detected [16]. As a result, the true extent of the damage may be underestimated by the segmentation process. The attenuation contrast can be enhanced by exploiting phase contrast [17]. X-ray micro-CT can be difficult to apply except on relatively small specimens because it is difficult to achieve high spatial resolution on large extended panels [11, 12]. Nevertheless, it has been regularly applied to determine [18–20] the extent and the complex layer-by-layer nature of the damage in CFRP arising from an impact load. Owing to the high level of detail of damage, which the X-ray CT can provide, it is often used as the ‘gold standard’ against which other cheaper and more accessible techniques, such as ultrasonic inspection, are compared and refined. Another advantage of the X-ray CT technique is that the high level of 3-D detail provides an excellent means of setting up microstructurally realistic, so-called image-based, models because it can be applied before, during and after testing to validate constitutive models of damage initiation and propagation in composites [21, 22]. Given the ease of making, and the difficulty of interpreting, ultrasound measurements of damage in polymer fibre-composites, it is perhaps surprising that relatively few side-by-side comparisons of ultrasound and X-ray CT measurements have been made to date [23], nor have models of the impact damage generally been validated in 3-D [24].

Thus, the strategy of the present paper is to use both the X-ray CT and ultrasonic C-scan techniques to assess the impact damage in a CFRP composite laminate that has been subjected to impact loading at a relatively low-velocity using a well-defined drop-weight test. One aim is to determine the ability of the two techniques to reveal damage in the same impacted CFRP test panel. Hence, a second aim is to identify the strengths and weaknesses of the two techniques. In addition, a third aim is to compare the experimental results to those predicted using a novel 3-D, elastic–plastic, FEA-based computational damage model that has recently been proposed [9].

2 Experimental Studies

2.1 Materials and Test Panels

The composite panels were made from unidirectional prepreg (MTC510-UD300-HS-33%RW) supplied by SHD Composites Ltd, UK. This prepreg contains an epoxy matrix (MTC510) and T700 carbon fibres at a fibre volume fraction of 60%. Flat panels were prepared using an autoclave and cut using a cut-off saw according to ASTM D7136 [25]. The prepreg was cured under a constant pressure of 6 bar with a 120 min dwell-time at 110 °C, using a 2 °C per minute temperature ramp. The glass transition temperature of the cured composite was 133 °C. The quasi-isotropic layup used for the panels was $[45_2/-45_2/0_2/90_2]_s$, where the 0° plies were aligned with the longer edge of the panels, which had a size of 150 mm × 100 mm, with a thickness, t , of 4.58 mm. In the figures below, the X-direction is defined as along the longer edge (i.e. 150 mm) and the Y-direction is defined as along the transverse shorter edge (i.e. 100 mm) of the panels.

2.2 Impact Tests

The CFRP panels were subjected to a low-velocity impact load using an Instron 9340 drop-weight tower supplied by CEAST, Italy, following the test method as described previously

[9]. A Boeing approved impact test rig was employed where the panels were held in place with four rubber clamps, one at each corner, over a fixture with a $125 \times 75 \text{ mm}^2$ cut-out window. A 16 mm diameter, stainless steel, round-nosed impactor, with an overall mass of 5.27 kg, was used to impact the panels with an impact energy of 7.5 J and a corresponding impact velocity of 1.69 m.s^{-1} . A catching system was used to prevent further impact events from occurring after the initial impact. No software filtering was applied to the load versus time data that was outputted and the accompanying software, provided by CEAST, produced both the impact load and the associated displacement of the panel as a function of time for the impact event. The displacement was determined by integration of the load versus time trace assuming Newton's second law. Duplicate experimental tests were undertaken and there was good agreement from these replicate tests.

The load versus time and load versus displacement responses for the rectangular composite panel, subject to the drop-weight impact test, are shown in Fig. 2. Relatively small amplitude, sinusoidal oscillations can be seen on the rising part of the load versus time, and the load versus displacement, experimental curves. These sinusoidal oscillations have previously been discussed in detail [9] and are indicative of mass-spring oscillations. On the experimental load versus time curve (red dashed line), there is a distinct load drop at a load of approximately 4.7 kN at a time of 1 ms, followed by oscillations indicative on the onset of damage initiation. This is also apparent on the load versus displacement curve. A duplicate test showed very similar behaviour. The predictions from the simulation numerical modelling (black solid line), see [9] and as discussed below, also show these effects; albeit the load at which damage initiation occurs in the model is somewhat lower. However, the overall response of the experimental load versus time and load versus displacement curves are very similar to those predicted from the modelling simulations. For example, for both the experimental and modelling results, the maximum load achieved is approximately 5 kN, the duration of impact event is approximately 4.6 ms and the overall displacement is approximately 2.5 mm.

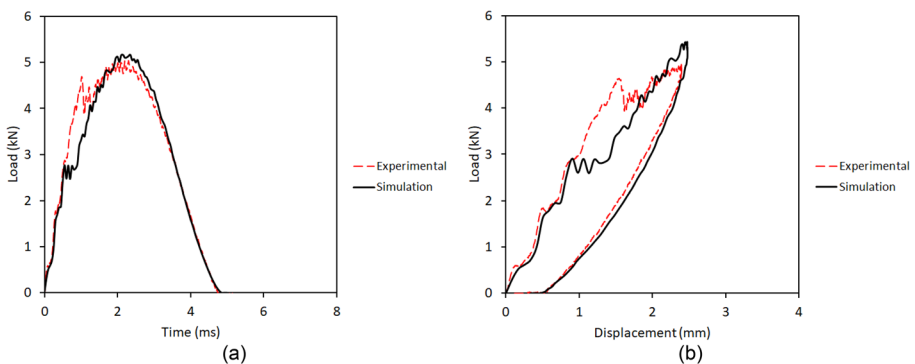


Fig. 2 The experimental and predicted load versus time and load versus displacement curves for the impacted CFRP panels. The red dashed line is a typical experimental test. A duplicate test showed similar behaviour. The black solid line shows the simulation prediction for load versus time and load versus displacement

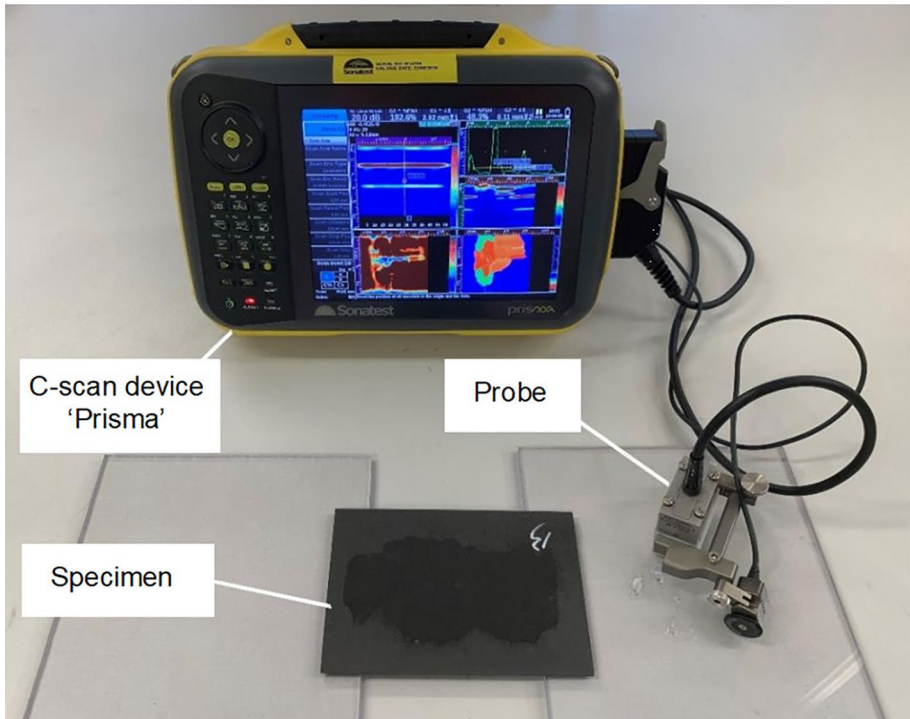


Fig. 3 Photograph of the ultrasonic C-scan equipment

2.3 The Ultrasonic C-Scan Inspection Technique

The impacted CFRP panels were inspected using a Prisma portable ultrasonic C-scanner supplied by Sonatest Ltd, UK, see Fig. 3, to detect any interlaminar damage that resulted from the impact loading. This technique has been discussed in detail elsewhere [9]. Essentially, a water spray is applied to the surface to act as a contact agent to ensure effective transmission of the ultrasonic waves from the transducer probe through the composite, using a scanning frequency of 5 MHz. These waves are reflected back to the transducer upon interacting with any delamination damage in the panel, and the position and size of the interlaminar damage can be determined from the total travel time and amplitude received by the transducer, respectively. The C-scanning equipment gave images with a scale from 0 to 4.58 mm, i.e. the thickness, t , of the panel. For this study, the reflection from the rear face of the panel was selected to be black so that all reflections from delaminations are coloured dark red through to dark blue. The total damage area was then calculated by counting the number of pixels that were not black in colour, since black corresponded to a region of the laminate free from interlaminar damage.

2.4 The X-ray Computed Tomography (CT) Technique

The impacted specimen was scanned at the University of Manchester using the Henry Moseley X-ray Imaging Facility's custom Nikon 225 kV X-ray tomography system ('High

Flux Bay'). The specimen from the impacted CFRP panel was sandwiched between two additional pieces of CFRP of the same type to help reduce scatter on the upper and lower surfaces of the specimen. The system was equipped with a 225 kV static tungsten reflection target source with a minimum focal spot size of 3 μm (at low wattage) and a PerkinElmer 4096 \times 4096 pixels 16-bit amorphous silicon flat-panel detector. The X-rays were generated using a voltage of 120 kV and a current of 88 μA (with power of 10.56 W). Each radiograph (projection) was acquired with an exposure time of 1000 ms, a gain of five, using binning of two, giving an effective detector size of 2048 \times 2048 pixels, with an effective pixel pitch of 200 μm . The total number of projections was 3181, which was fixed using an optimisation based on the Nyquist–Shannon sampling theorem. Eight frames were taken per projection giving an approximate total scan time of 7 h per scan. The specimen was scanned twice at two different resolutions, using the same X-ray and exposure settings, giving two data sets with isotropic pixels sizes of 27 μm and 17 μm . The 3-D volumes were reconstructed from the projection data at full resolution as 16-bit tiff stacks using Nikon's 'CT Pro 3-D software', supplied by Nikon X-Tek Systems Ltd, UK. Orthogonal CT slices from the tomogram are shown in Fig. 4 of the central disc containing the impact damage.

The software FIJI-ImageJ [26] was first used to reorientate the data from the arbitrary angle at which the CT scanning was performed. This allowed orthogonal slices in the data to align with the 0° and 90° plies. The software 'Avizo 2020.2', supplied by ThermoFisher Scientific, UK, was used for the rest of the image processing and data visualisation. The primary data used for the analysis was the dataset with a pixel size of 17 μm . The dataset at 27 μm pixel size was initially analysed with the procedure to be described below but it was

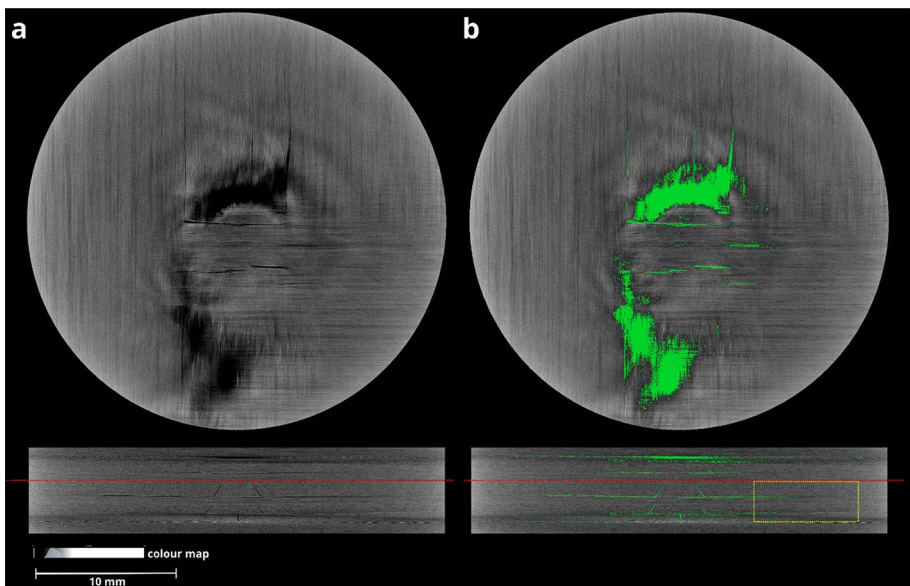


Fig. 4 Orthogonal regions of interest (at the same scale) taken from the X-ray CT data X–Y (top) and X–Z (bottom) slices: **a** prior to segmentation and **b** with the segmentation of the damage (rendered green) superimposed on the 17 μm pixel size dataset. The red dashed lines show the location of the other orthogonal slice. The yellow box region is referred to in Fig. 7. (The X-ray CT scan is performed on a central disc taken from the rectangular specimen.)

found that the lateral extent of the segmented damage was confined within the field of view scanned by the 17 μm dataset. When directly comparing the two datasets, it was evident that many of the fine features had not been resolved in the 27 μm dataset. Therefore, even if the lateral extent of the damage region did extend beyond the 17 μm dataset, those features would not have been resolved. (The issue of partial volume effects and limitations of the segmentation of the CT data is highlighted again later in Section 3.4 and Fig. 7).

Segmentation of the crack surfaces was important to characterise and highlight the damage in the composite laminate. This was undertaken with a semi-automated approach. The low- and high-resolution datasets were aligned in the ‘Avizo 2020.2’ software to give a full overview of the specimen. The data was then trimmed to exclude the extra CFRP that the specimen was sandwiched between. As well as, in the case of the 17 μm dataset, to exclude edge artifacts arising from performing an internal tomography scan and from uncorrected beam-hardening artefacts. The data were thresholded based on a grey-scale attenuation value into two regions: the fracture region and the rest of the composite. Manual adjustment was made to include as much of the delaminations and other fractures as possible, while ensuring that as little undamaged composite was accidentally captured in the analysis. (This is a requirement due to the attenuation overlap between the lowest attenuating composite and the finest fracture regions.) No image filters were applied to the data prior to histogram segmentation. After thresholding the data, a ‘remove small spots’ function was used in the X–Y direction (parallel to the delaminations). This was set to remove isolated regions of segmentation data of 10 pixels, or less, in area. This pixel size was chosen after iteratively testing other sizes until the majority of the segmented regions that were removed were due to noise that was clearly located within the ply, and not at boundaries or fractures. This segmented data has been overlaid as a ‘Colour Wash’ in several of the figures in this paper including Figs. 4, 7 and 8. For 3-D rendering, the segmented data was manually separated into layers either by highlighting the data slice-by-slice or by using the ‘3-D lasso tool’ in the software. The motivation behind the analysis method was to alter the raw image data as little as possible so as to reduce information loss via feature blurring, such as using median filtering, when removing data noise. Instead, noise was removed from the resulting segmentation data, instead of segmenting data with removed noise.

2.5 Modelling Methodology

A 3-D, elastic–plastic (E-P), finite element analysis (FEA) numerical damage model has been previously developed and verified [9, 27, 28] for predicting interlaminar, intralaminar and other damage processes, such as a permanent plastic indentation in the composite panel caused by the impactor, when subjected to an impact load. Indeed, in the present work, the model has already been shown to be able to predict quite accurately the overall response of the experimental load versus time and load versus displacement curves, see Fig. 2. Thus, next, its ability to predict the type, location and extent of the impact damage introduced into the composite CFRP panel is assessed by comparing the simulation results to the experimental results from the C-scan and X-ray CT techniques. The FEA model was implemented in ‘Abaqus 2020’ (Dassault Systemes, France) and the overall flow chart is shown in Fig. 5 for the main model and the E-P model, which was incorporated as a user-defined material (‘VUMAT’) sub-routine into the main FEA code. This flow-chart provides the sequence of the modelling steps and the relevant equation numbers, as previously given and explained in [9]. The flow-chart in Fig. 5, together with reference [9], allows the reader to follow the logical computational sequence of the numerical model: including

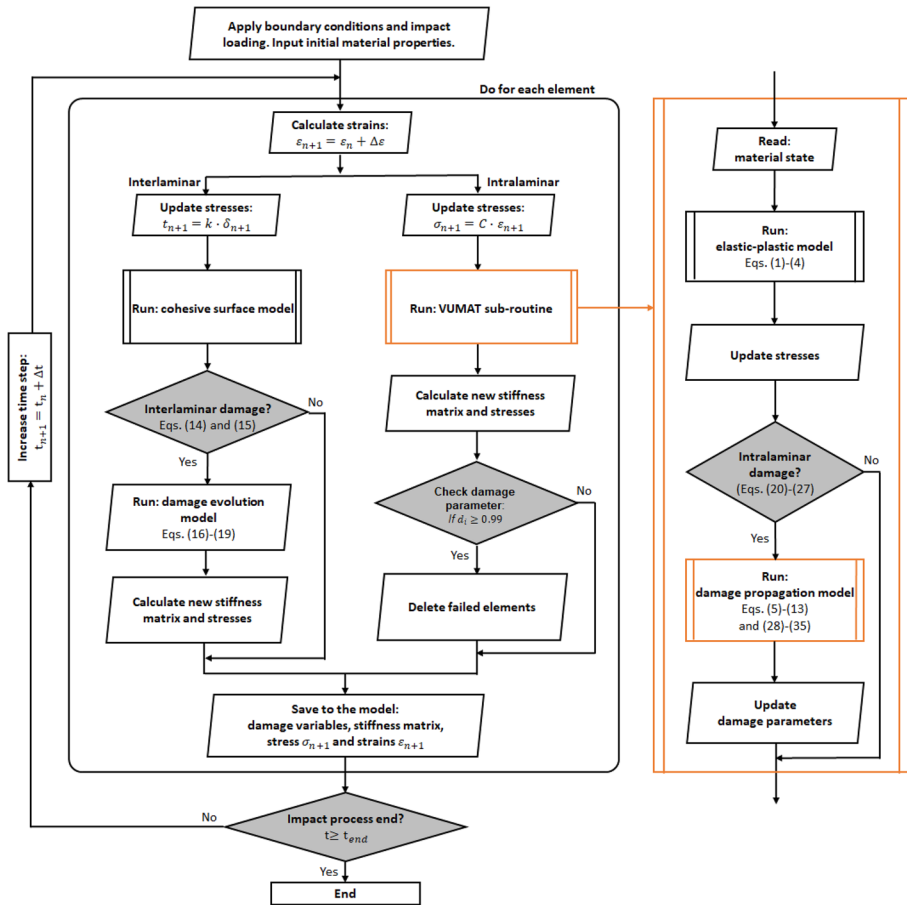


Fig. 5 The implementation of the E-P, 3-D FEA numerical damage model showing schematically the overall flowchart for one computational time-step and a single integration point. Both the flowcharts for the main model and for the elastic–plastic (E-P) user-defined sub-routine are shown. This FEA modelling simulation of the impact event would be run typically over a timescale, t , of 0 to ca. 8 ms, with ca. 100 time-steps being employed. The simulation runs were stopped when the defined total computation time for the impact simulation event had expired. (All the methodologies and equations that are used in the above FEA model are derived and presented in [9], where the equations are numbered as above.)

the novel E-P model, the failure criteria used and how crack initiation and propagation for the intralaminar and interlaminar damage regions are defined and quantitatively modelled. For the modelling studies the basic mechanical properties of the composite plies, including strength, modulus, Poisson’s ratio and fracture toughness, etc., that are required for the modelling simulation were obtained from the manufacturer’s data sheets and from the literature [9, 27] and are given in Table 1.

Table 1 The properties, as defined by the terminology given in [9], of a unidirectional CFRP ply used in the FEA modelling studies [9, 27]

Property	CFRP
Moduli (GPa)	$E_{11} = 115; E_{22} = E_{33} = 8.2$ $G_{23} = 3.6; G_{12} = G_{13} = 3.6$
Poisson's ratio	$\nu_{23} = 0.34; \nu_{12} = \nu_{13} = 0.34$
Strength, S , values (MPa)	$S_{1t} = 2282; S_{2t} = S_{3t} = 54$ $S_{1c} = 1067; S_{2c} = S_{3c} = 200$ $S_{12} = S_{13} = S_{23} = 99$
Intralaminar ply fracture energies (kJ/m ²)	$G_{Ic} _{ft} = 133; G_{Ic} _{fc} = 40$ $G_{Ic} _{mt} = 0.4; G_{Ic} _{mc} = 1.3; G_{IIc} _{ms} = 1.3$
Interlaminar ply fracture energies (kJ/m ²)	$G_{Ic} = 0.4; G_{IIc} = 1.3$
Benzeggagh–Kenane exponent	$\eta = 1.45$
Cohesive strengths (MPa)	$t_{33}^0 = 43.0; t_{31}^0 = t_{32}^0 = 50.0$
Initial cohesive law stiffness (MPa/mm)	$k_i = 6.4 \times 10^5$
E-P model: coefficient, a_{66} , and material constants, A and n	$a_{66} = 2.7; A = 3.14 \times 10^{-13} \text{ MPa}^{-n};$ $n = 4.19$

3 Results and Discussion

3.1 Introduction

The damage maps from the C-scan and X-ray computed tomography (CT) experimental techniques, and from the numerical simulation predictions, for the delamination footprint, with the associated damage area (labelled ‘DA’), are presented in Fig. 6. The rear surface was selected to be black so that delaminations at different depths through the thickness of the specimen would be more clearly visible. The 0° fibre direction is along the X-direction, i.e. the longest edge of the rectangular 150 × 100 mm specimen. The areal footprint of the damage, i.e. the damage area (labelled ‘DA’), is given at the top left in each case and this

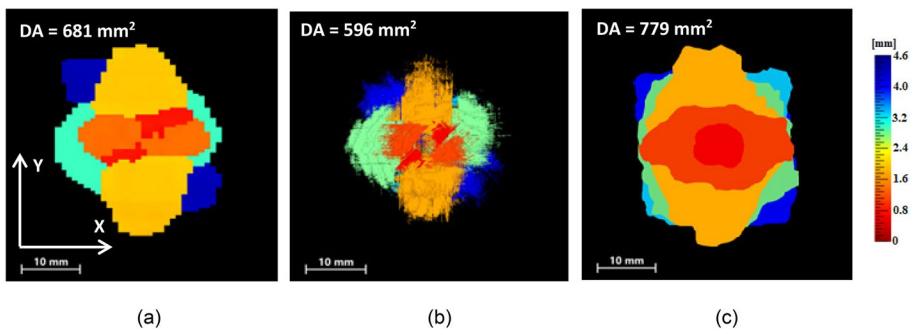


Fig. 6 Typical damage maps in the X–Y plane from **a** the experimental ultrasonic C-scan inspection technique, **b** the experimental X-ray CT technique and **c** the numerical modelling predictions. The impact was on the top surface and the layers are colour-coded from the top (red) surface to the bottom (black) as indicated by the damage depth colour bar

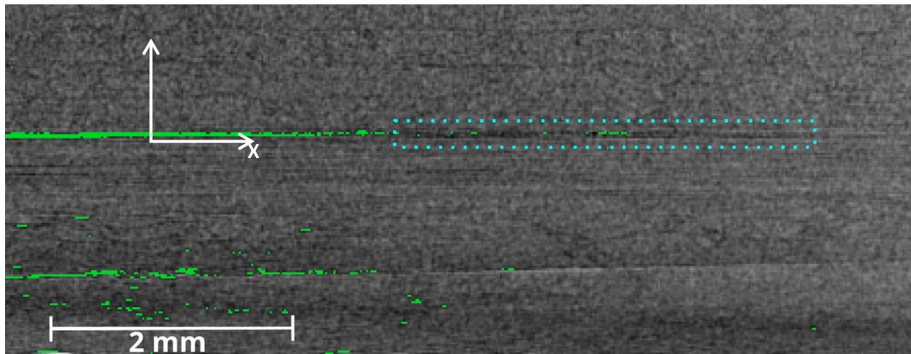


Fig. 7 Enlarged region taken from the edge of the damaged zone in the black and white CT slice in Fig. 4 (indicated by the yellow box) showing the tendency for the segmentation to underestimate the extent of the delamination observed. The dashed-cyan outlined box shows the discontinuous segmentation at the delamination front. Although a linear damage feature can be seen by eye, the change in attenuation and decrease in contrast between the fracture and the background composite makes the feature extremely difficult to segment automatically

was determined by counting the number of pixels which had a colour that was not black for the damage footprint as a whole as viewed from the top surface. (Delaminations overlap so the total area of delamination between plies would be higher but the delamination footprint is considered as a good indicator of the areal extent of damage.)

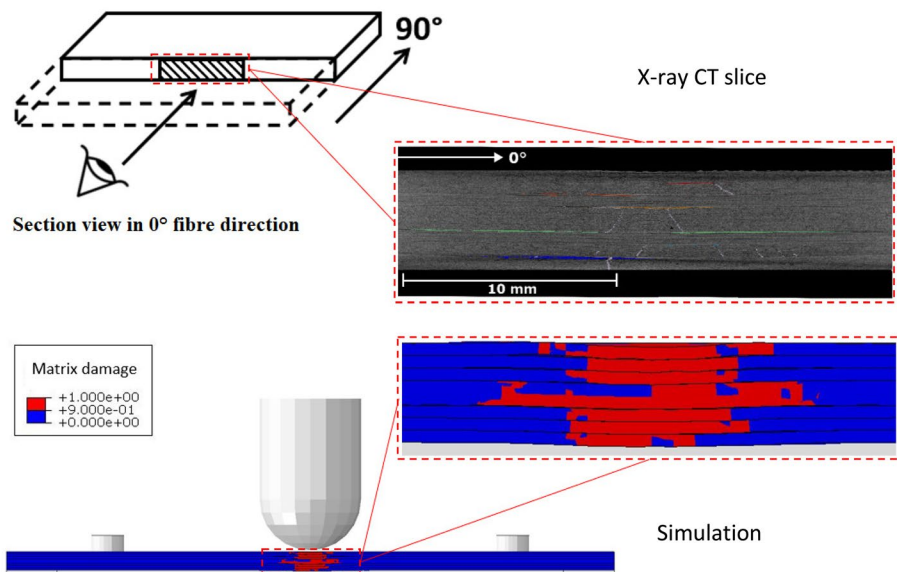


Fig. 8 Intralaminar damage along the 0° fibre direction, comparing the results from the experimental X-ray CT technique with those from the numerical modelling studies. (The text box shows that the value of the damage parameter for intralaminar damage to be initiated in the modelling studies was taken to be equal to, or greater, than 0.9 [9].)

3.2 Damage Maps Obtained by Ultrasonic C-Scan Inspection

The C-scan damage map in Fig. 6(a) is based on ultrasonic wave reflection with a transducer and detector on the upper surface. This process can detect very accurately any separation, i.e. delamination, between the ply interfaces. However, the C-scan spatial resolution is about 1 pixel per mm² and this is evident in the pixelated nature of the C-scan image.

Now, the given damage area was determined for interlaminar damage, i.e. delaminations, in the CFRP panel resulting from the impact event, as shown in Fig. 6. Delaminations initiate and grow at interfaces where the fibre direction is different in the plies below and above the interface. The propagation of the delamination is dominated by the fibre direction of the ply furthest from the impact surface. Localised deformation drives the initiation of matrix cracking and subsequent delamination. Due to the changes in stiffness across the interface between composite plies in different directions, the interfacial shear stresses can drive the crack growth mainly in Mode II (or shear loading) to form a larger delamination area. As the composite specimen has a symmetric layup of $[45_2/-45_2/0_2/90_2]_s$, the interfaces at each change of fibre orientation initiate delaminations which grow in the direction of the fibre on the lower ply, and this gives the characteristic delamination rosette, seen in Fig. 6(a).

3.3 Damage Maps Obtained by X-ray Computed Tomography (CT)

It should be remembered that the physical process by which the delaminations are observed in X-ray CT is fundamentally different from that in the C-scan ultrasonic technique. The latter technique is very sensitive to loss of contact as this provides a sharp change in acoustic impedance and a strong reflection. As a result, the surfaces could be of the order of 1 μm apart, or less, and an ultrasonic reflection would still occur. However, X-ray CT is based on density and composition changes, as well as atomic number, which affect the attenuation, within each pixel. Thus, X-ray CT only shows significant attenuation contrast when the separation of the two surfaces is sufficiently far apart to change significantly the amount of material, and hence the attenuation, within a pixel. The primary dataset pixel size in this X-ray CT study, was 17 μm and at this resolution a very fine crack or delamination with a separation less than a pixel is unlikely to be detected because of the low contrast between air and the composite [16]. However, where the crack opening was greater than a pixel, e.g. in the striations towards the boundary of the delamination, the separation between the laminae

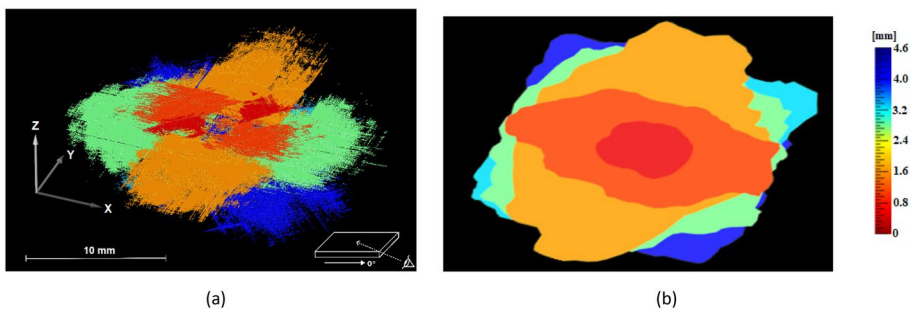


Fig. 9 Interlaminar damage in a 3D view, comparing the results from **a** the experimental X-ray CT technique and **b** the numerical modelling predictions. The impact was on the top surface and the layers are colour-coded from the top (red) surface to the bottom (black) as indicated by the colour bar

surfaces is sufficient for a delamination to be clearly visible. This is exacerbated by the automated segmentation process which is conservative in segmenting the cracks, often requiring multiple pixel widths to be affected before assigning a crack, so as not to be too sensitive to noise [15]. This tendency to underestimate the lateral extent of delamination is evident in the enlarged region of interest taken from Fig. 4 and shown in Fig. 7. The results shown in Fig. 6(a) and (b), as well as in Fig. 9(a) and (b) to be shown later, do indeed confirm the above comments in that there is a tendency for the X-ray CT technique to underestimate the lateral extent of the area of delamination compared to the C-scan technique. Interestingly, this has been observed previously [18, 19, 29] but not discussed in detail.

Nevertheless, the orientation and relative size of the delaminations, at the respective interfaces, of the composite laminate are very similar from both techniques, see Fig. 6(a) and (b) which have similar colour coding to show the depth of the delamination through the thickness of the composite specimen. In Fig. 6(b) the results from the X-ray CT scan reveal that the striations and other features indicate very clearly that the delaminations are growing in the direction of the plies beneath each ply interface. Figure 6(a) for the C-scan image identifies the delaminations in the same locations through the depth of the composite as the results from the X-ray CT scan and also confirms that the delaminations are growing in the direction of the plies beneath each ply interface. Figure 6(a) for the C-scan and Fig. 6(b) for the X-ray CT scan both show a similar characteristic rosette indicative of the delaminations, observed at the ply interfaces, for the fibre layup of $[45_2/-45_2/0_2/90_2]_s$. Thus, the overall shape and locations of the delaminations are very similar as determined from both the X-ray CT and the ultrasonic C-scan inspection techniques. However, the detail and resolution of the X-ray CT image are much sharper than for the C-scan image, as would be expected.

Finally, one feature seen in the X-ray CT data that is not evident in the C-scan data, and is apparent in the modelling simulation (see below), is the presence of distinct intralaminar matrix cracking. This can be best seen in the cross-section in Fig. 4 (in the lower images), Fig. 7 and the coloured X-ray CT slice in Fig. 8. Matrix cracking is expected to result from the present impact tests and a detail to note is where the lateral extent of the delaminations are abruptly terminated by linear features that are angled relative to the longitudinal fibre direction in the adjacent ply. These linear features are intralaminar matrix fractures that cross-cut the matrix at approximately 45° to the plane of the ply, as may be seen in the cross-sections in Fig. 4 (in the lower images) and Fig. 8. This suggests a mechanism of energy transfer down and laterally through the impacted specimen.

3.4 Damage Maps Obtained by Numerical Modelling

Figure 6(c) shows the results from the numerical modelling simulations for the delamination damage and a delamination rosette is predicted from these studies with all the features observed from the experimental ultrasonic C-scan and X-ray CT techniques, see Fig. 6(a) and (b) respectively. This is with delaminations occurring at the interfaces between plies and growing in the fibre direction below the ply interface. The overall delamination damage area (DA) appears to be slightly overestimated in Fig. 6(c) but when considering the complexity of the damage processes involved, and the fact that all the main processes of the impact event and damage are captured in the model without any fitting factors, it is considered that the predictions are in very reasonable agreement with the experimental results.

Figure 8 shows an X-ray CT section with intralaminar matrix cracking clearly visible. This is compared with the intralaminar matrix cracking as predicted by the numerical modelling

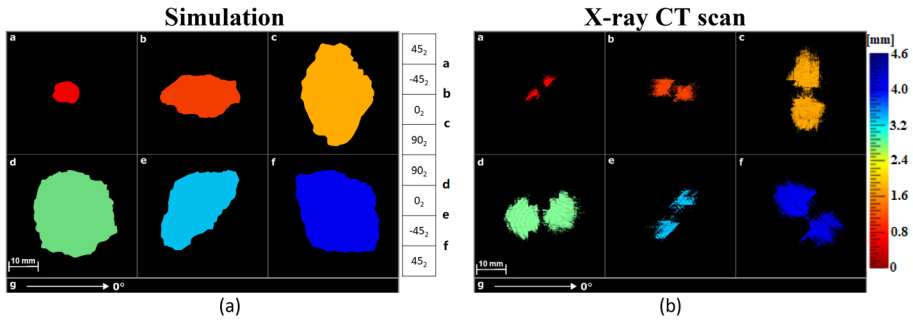


Fig. 10 Interlaminar damage between blocking plies, comparing the results from **a** the numerical modelling with those from **b** the experimental X-ray CT scan

studies and there is good agreement with respect to the extent and location of the intralaminar matrix cracking. Again, it should be noted that the ultrasonic C-scan technique used is not able to detect matrix cracking, so this is a clear advantage of the X-ray CT imaging technique.

Figure 9 compares the experimental X-ray CT data and the predictions from the numerical modelling studies from an isometric viewpoint and illustrates more clearly the orientation of the interlaminar delaminations through the thickness. As described above, striations that are visible in Figs. 6(b) and 9(a), occur where the separation of the delamination is sufficient to give significant change in the attenuation within the measurement voxel. These striations follow the fibre direction in the lower layer. The overall shape and locations of the delaminations are very similar as determined from both the experimental X-ray CT technique (Fig. 9(a)) and the numerical modelling predictions (Fig. 9(b)).

Figure 10 shows the damage numerically predicted and experimentally recorded for the X-ray CT scan for delamination at each of the interfaces between differently oriented plies through the thickness of the composite panel for the present CFRP layup of 45₂, -45₂, 0₂, 90₂, 90₂, 0₂, 45₂, 45₂. The numerical prediction, in Fig. 10(a), shows that delaminations tend to grow in the fibre direction that is present below the interface. For comparison, the experimental X-ray CT scan delamination map is shown in Fig. 10(b) and there is good agreement with the simulation results with respect to the shape and location of such interlaminar damage, although again the experimental X-ray CT technique does appear to underestimate the areal extent of the delaminations.

4 Conclusions

Low-velocity impact damage in composite laminates is typically barely visible to the naked eye. However, the techniques of ultrasonic C-scan and X-ray computed tomography (CT) can detect sub-surface impact damage in composite laminates. Both interlaminar and intralaminar damage can occur in laminates. This is with interlaminar damage taking the form of delaminations between the plies and intralaminar damage, e.g. matrix cracking, occurring in the matrix of the ply itself. The ultrasonic C-scan method is very effective at revealing delaminations between plies, as these are usually perpendicular to the direction of travel of the ultrasound. However, ultrasound does not very readily detect intralaminar matrix cracking in the composite. The pixel size in the ultrasound C-scan technique is quite coarse at about 1 mm and so the sub-surface damage footprint of the delaminations often

appears pixelated but these delaminations can be colour-coded to show their depth through the laminate panel.

The X-ray computed tomography (CT) technique provides much finer detail of the sub-surface impact damage within a composite laminate, particularly when a voxel or pixel size of 17 μm is employed. However, even at this fine pixel size, owing to the nature of the attenuation being a function of atomic number and material density, it is still possible for a very fine crack or delamination, of the order of 1 μm separation, to be missed. When the crack opening was greater than a 17 μm pixel size, e.g. in the striations towards the boundary of the delamination, the separation between the composite ply surfaces is sufficient for a delamination to be clearly visible. The X-ray CT scans can also be colour-coded to show the depth of delaminations. The X-ray computed tomography (CT) technique is particularly good at revealing matrix cracking, i.e. intralaminar damage. Matrix cracks often connect delaminations, at neighbouring interfaces, by cutting across the matrix at approximately 45° to the specimen surface. This is thought to be due to a mechanism of energy transfer down and laterally through the specimen. Methods to improve feature detection and segmentation can be approached either via alternative imaging, or advanced segmentation, methods. In the case of segmentation, one approach could be utilising the development of machine learning algorithms such as Trainable Weka Segmentation [30] and software packages such as IPDSK (Reactiv'IP, Grenoble) [31] and DragonFly (Comet, Montréal) [32]. These software could provide a semi-automated approach to segmentation. This would be more appropriate for larger datasets with multiple samples to justify the initial time investment to create the training datasets. Regarding providing alternative imaging methods, one option could be to employ Phase-contrast Imaging [33, 34] to enhance the boundaries between materials (in this case, polymer and air). However, for this study, the samples were not suitable for this imaging method with the equipment available. Future studies would need to plan using this method of imaging at the sample preparation stage.

The numerical 3-D finite-element analysis (FEA) model, with an elastic–plastic (E-P) user-defined sub-routine, predicts all the effects observed in the X-ray computed tomography and ultrasonic C-scan techniques. The FEA model can predict the position and orientation of interlaminar delaminations in detail through the thickness of the laminate and it can also show where there is expected to be intralaminar matrix cracking. The predictions agreed very well with the experimental observations from the ultrasonic C-scan and X-ray computed tomography (CT) techniques.

The main conclusions to be drawn are:

- The ultrasonic C-scan method is very effective at revealing delamination between plies, after impact on composite laminates. However, the image is pixelated with pixel size of 1 mm.
- The X-ray computed tomography (CT) technique is particularly good at revealing matrix cracking, i.e. intralaminar damage and in general much more detail is obtained, with a pixel size down to 17 μm .
- Methods to improve feature detection and segmentation for X-ray CT are possible in the future, using machine learning and other techniques.
- A numerical 3-D finite-element analysis (FEA) model, with an elastic–plastic (E-P) user-defined sub-routine, can predict delamination and matrix cracking in composite laminates after impact.

Acknowledgements The manufacture of composite panels by Professor Lee Harper and Dr. Adam Joesbury, Composites Research Group, University of Nottingham is very much appreciated. The X-ray imaging beamtime for this study was kindly provided through funding from the National Research Facility for Laboratory-based X-ray CT (NXCT) EPSRC grant EP/T02593X/1. It took place within the Henry Moseley

X-ray Imaging Facility (HMXIF), which was established through EPSRC grants EP/F007906/1, EP/I02249X/1 and EP/F028431/1. HMXIF is also a part of the Henry Royce Institute for Advanced Materials, established through EPSRC grants EP/R00661X/1, EP/P025498/1 and EP/P025021/1. For the purpose of open access, the authors have applied a Creative Commons Attribution (CC BY) license to any Author Accepted Manuscript version.

Data Availability The datasets are available from the corresponding authors on reasonable request.

Declarations

Competing Interest The authors declare that they have no known competing financial interests or personal relationships that could have appeared to influence the work reported in this paper.

Open Access This article is licensed under a Creative Commons Attribution 4.0 International License, which permits use, sharing, adaptation, distribution and reproduction in any medium or format, as long as you give appropriate credit to the original author(s) and the source, provide a link to the Creative Commons licence, and indicate if changes were made. The images or other third party material in this article are included in the article's Creative Commons licence, unless indicated otherwise in a credit line to the material. If material is not included in the article's Creative Commons licence and your intended use is not permitted by statutory regulation or exceeds the permitted use, you will need to obtain permission directly from the copyright holder. To view a copy of this licence, visit <http://creativecommons.org/licenses/by/4.0/>.

References

1. Roeseler, W.G., Sarh, B., Kismarton, M.U.: Composite structures: the first 100 years. Proc. Int Conf. Compos. Mater., Kyoto, Japan, 1–4 (2007)
2. Soutis, C.: Fibre reinforced composites in aircraft construction. Prog. Aerospace Sci. **41**, 143–151 (2005)
3. Falzon, B.G., Pierce, R.S.: Thermosetting composite materials in aerostructures. In Revolutionizing Aircraft Materials and Processes, Eds. S. Pantelakis and K. Terpes, Springer, CH, 57–86 (2020)
4. Caminero, M.A., García-Moreno, I., Rodríguez, G.P.: Damage resistance of carbon fibre reinforced epoxy laminates subjected to low velocity impact: Effects of laminate thickness and ply-stacking sequence. Polym. Test. **63**, 530–541 (2017)
5. Zimmermann, N., Wang, P.H.: A review of failure modes and fracture analysis of aircraft composite materials. Eng. Fail. Anal. **115**, 104692 (2020)
6. Park, H., Kong, C.: Experimental study on barely visible impact damage and visible impact damage for repair of small aircraft composite structure. Aerospace Sci. Tech. **29**, 363–372 (2013)
7. Cantwell, W.J., Morton, J.: The impact resistance of composite materials - a review. Composites **22**, 347–362 (1991)
8. Batra, R.C., Gopinath, G., Zheng, J.Q.: Damage and failure in low energy impact of fiber-reinforced polymeric composite laminates. Compos. Struct. **94**, 540–547 (2012)
9. Liu, H., Liu, J., Ding, Y., Hall, Z.E., Kong, X., Zhou, J., Blackman, B.R.K., Kinloch, A.J., Dear, J.P.: A three-dimensional elastic-plastic damage model for predicting the impact behaviour of fibre-reinforced polymer-matrix composites. Compos. Part B **201**, 108389 (2020)
10. Davies, G.A.O., Olsson, R.: Impact on composite structures. Aeronaut. J. **108**, 541–563 (2004)
11. Rus, J., Gustschin, A., Mooshofer, H., Grager, J.-C., Bente, K., Gaal, M., Pfeiffer, F., Grosse, C.U.: Qualitative comparison of non-destructive methods for inspection of carbon fiber-reinforced polymer laminates. J. Compos. Mater. **54**, 4325–4337 (2020)
12. Garcea, S.C., Wang, Y., Withers, P.J.: X-ray computed tomography of polymer composites. Compos. Sci. Tech. **156**, 305–319 (2018)
13. Bull, D.J., Helfen, L., Sinclair, I., Spearing, S.M., Baumbach, T.: A comparison of multi-scale 3D X-ray tomographic inspection techniques for assessing carbon fibre composite impact damage. Compos. Sci. Technol. **75**, 55–61 (2013)
14. Leonard, F., Stein, J., Soutis, C., Withers, P.J.: The quantification of impact damage distribution in composite laminates by analysis of X-ray computed tomograms. Compos. Sci. Technol. **152**, 139–148 (2017)

15. Withers, P.J., Bouman, C., Carmignato, S., Cnudde, V., Grimaldi, D., Hagen, C.K., Maire, E., Manley, M., Du Plessis, A., Stock, S.R.: X-ray computed tomography. *Nat. Rev. Methods Primers* 1–18 (2021)
16. Yu, B., Bradley, R.S., Soutis, C., Withers, P.J.: A comparison of different approaches for imaging cracks in composites by X-ray microtomography. *Phil. Trans. R. Soc. A* **374**, 20160037 (2016)
17. Shoukroun, D., Massimi, L., Iacoviello, F., Endrizzi, M., Bate, D., Olivo, A., Fromme, P.: Enhanced composite plate impact damage detection and characterisation using X-Ray refraction and scattering contrast combined with ultrasonic imaging. *Compos. Part B* **181**, 107579 (2020)
18. Katunin, A., Wronkowicz-Katunin, A., Dragan, K.: Impact damage evaluation in composite structures based on fusion of results of ultrasonic testing and x-ray computed tomography. *Sensors* **20**, 1867 (2020)
19. Lu, T., Chen, X., Wang, H., Zhang, L., Zhou, Y.: Comparison of low-velocity impact damage in thermoplastic and thermoset composites by non-destructive three-dimensional X-ray microscope. *Polym. Test.* **91**, 106730 (2020)
20. Suvarna, R., Arumugam, V., Bull, D.J., Chambers, A.R., Santulli, C.: Effect of temperature on low velocity impact damage and post-impact flexural strength of CFRP assessed using ultrasonic C-scan and micro-focus computed tomography. *Compos. Part B* **66**, 58–64 (2014)
21. Sencu, R.M., Yang, Z., Wang, Y.C., Withers, P.J., Rau, C., Parson, A., Soutis, C.: Generation of micro-scale finite element models from synchrotron X-ray CT images for multidirectional carbon fibre reinforced composites. *Compos. Part A* **91**, 85–95 (2016)
22. Sencu, R.M., Yang, Z., Wang, Y.C., Withers, P.J., Soutis, C.: Multiscale image-based modelling of damage and fracture in carbon fibre reinforced polymer composites. *Compos. Sci. Technol.* **198**, 108243 (2020)
23. Thorsson, S.I., Waas, A.M., Rassaian, M.: Low-velocity impact predictions of composite laminates using a continuum shell based modeling approach Part b: BVID impact and compression after impact. *Int. J. Solids Struct.* **155**, 201–212 (2018)
24. Katunin, A., Wronkowicz-Katunin, A., Danek, W., Wyleźół, M.: Modeling of a realistic barely visible impact damage in composite structures based on NDT techniques and numerical simulations. *Compos. Struct.* **267**, 113889 (2021)
25. ASTM D7136.: Standard test method for measuring the damage resistance of a fiber-reinforced polymer matrix composite to a drop-weight impact event. Philadelphia, PA, USA (2012)
26. Rasband, W.S.: ImageJ, U. S. National Institutes of Health, Bethesda, Maryland, USA. <https://imagej.net/ij/index.html>
27. Liu, H., Brooks, R.A., Hall, Z.E.C., Liu, J., Crocker, J.W.M., Joesbury, A.M., Harper, L.T., Blackman, B.R.K., Kinloch, A.J., Dear, J.P.: Experimental and numerical investigations on the impact behaviour of pristine and patch-repaired composite laminates. *Phil. Trans. R. Soc. A* **380**, 20210340 (2022)
28. Liu, H., Liu, J., Hall, Z.E.C., Brooks, R.A., Crocker, J.W.M., Joesbury, A.M., Harper, L.T., Blackman, B.R.K., Kinloch, A.J., Dear, J.P.: Modelling the effects of patch-plug configuration on the impact performance of patch-repaired composite laminates. *Compos. Sci. Technol.* **233**, 109917 (2023)
29. Wronkowicz, A., Dragan, K., Lis, K.: Assessment of uncertainty in damage evaluation by ultrasonic testing of composite structures. *Compos. Struct.* **203**, 71–84 (2018)
30. Arganda-Carreras, I., Kaynig, V., Rueden, C., Eliceiri, K.W., Schindelin, J., Cardona, A., Sebastian, S.H.: Trainable Weka Segmentation: a machine learning tool for microscopy pixel classification. *Bioinformatics* **33**, 2424–2426 (2017)
31. Bernard, L.: Reactiv'IP SAS, Montréal, Québec, France. <https://www.reactivip.com>
32. Dragonfly, Comet Technologies Canada Inc., Grenoble, Canada. <https://www.theobjects.com>
33. Endrizzi, M.: X-ray phase-contrast imaging. *Nucl. Instrum. Methods Phys. Res. Sect. A: Accelerators Spectrometers, Detectors and Associated Equipment* **878**, 88–98 (2018)
34. Mayo, S.C., Stevenson, A.W., Wilkins, S.W.: In-line phase-contrast x-ray imaging and tomography for materials science. *Mater* **5**, 937–965 (2012)

Publisher's Note Springer Nature remains neutral with regard to jurisdictional claims in published maps and institutional affiliations.